Eur. Phys. J. B **50**, 565–569 (2006)
DOI: 10.1140/epjb/e2006-00180-3

THE EUROPEAN PHYSICAL JOURNAL B

Flux trapping in a macroscopic cylinderical hole drilled in Bi-Sr-Ca-Cu-O

A. Kiliç[1,a], K. Kiliç[1], H. Yetiş[1], M. Olutaş[1], A. Altinkok[1], H. Sözeri[2], and O. Çetin[1]

[1] Abant Izzet Baysal University, Department of Physics, Turgut Gulez Research Laboratory, 14280 Bolu, Turkey
[2] National Metrology Institute TUBITAK P.O. Box 21, 41470, Gebze-Kocaeli, Turkey

Received 7 December 2005 / Received in final form 4 March 2006
Published online 17 May 2006 –

Abstract. The flux dynamics in a polycrystalline sample of $Bi_{1.7}Pb_{0.3}Sr_2Ca_2Cu_3O_x$ with a macroscopic cylindrical hole (CH) drilled was investigated by slow transport relaxation ($V-t$ curves) and magneto-voltage measurements ($V-H$ curves). It was monitored that there are several discontinuities in the time evolution of quenched state in $V-t$ curves, which was attributed to the leaving of quantized flux lines trapped through CH together with surface superconducting effects. We observed that asymmetric $V-H$ curves demonstrate unusual remarkable counter clockwise hysteresis effects upon cycling of field. This interesting result was correlated mainly to the flux trapping inside the CH that acts as a macroscopic attractive pinning center for flux lines. Further, the hysteresis effects in $V-H$ curves for a fixed transport current provide a direct evidence that the number of flux lines, measured dissipation and relative decrease/increase in irreversibilities could be determined by sweeping rate of external magnetic field (dH/dt) which leads also to peculiar time effects.

PACS. 74.72.Hs Bi-based cuprates – 74.25.Qt Vortex lattices, flux pinning, flux creep

1 Introduction

In type-II superconductors, the flux dynamics is governed by two competing physical mechanisms, attractive interaction between flux lines and pinning centers which are randomly distributed inside the sample, and repulsive interaction of flux lines which favors order [1,2]. In order to increase their pinning properties, artificial columnar defects can be produced by heavy-ion irradiation [3,4], which can cause considerably an enhancement in the pinning efficiency and current carrying capacity of the material. In addition, the advances in lithographic techniques allow to fabricate antidotes which act as strong pinning centers under suitable conditions [5–7]. For instance, it is possible to fabricate well ordered arrays of columnar defects in superconducting thin films with radius comparable to coherence length ξ by using high resolution of electron beam lithography technique [6]. Matching between the regular array of columnar defects and the flux line lattice can be obtained by adjusting the external magnetic field being in the form of integer multiple or some fraction of matching fields, i.e., commensurability effects [6].

The aim of this study is to investigate the time dependent flux motion in a polycrystalline sample of $Bi_{1.7}Pb_{0.3}Sr_2Ca_2Cu_3O_x$ (BSCCO) drilled cylindrical hole (CH) with a diameter of 0.5 mm. We present the results of slow transport relaxation ($V-t$ curves) and magnetovoltage ($V-H$ curves) measurements with different sweeping rate (dH/dt) of external magnetic field in a polycrystalline sample of $Bi_{1.7}Pb_{0.3}Sr_2Ca_2Cu_3O_x$ (BSCCO) drilled cylindrical hole (CH) with a diameter of 0.5 mm. Several discontinuities observed in the time evolution of quenched state of the $V-t$ curves are interpreted in terms of leaving of quantized flux lines through CH. We show that dH/dt becomes an important parameter in the evolution of $V-H$ curves, which determines the measured dissipation and degree of relative irreversible effects. For different values of dH/dt, pronounced counter clockwise hysteresis effects appearing in asymmetric $V-H$ curves is considered as a direct evidence of flux trapping in CH that sets an attractive potential energy for flux lines. The results are compared to those of similar measurements performed on the same BSCCO sample before drilling of CH. Finally we suggest that investigation of such a macroscopic CH via $V-t$ and $V-H$ curves will provide a direct contribution to designing of superconducting quantum interference devices (SQUIDs). In these devices, a few strategically introduced holes can trap the vortices and reduce profoundly the noise by increasing their performance.

2 Experiment

$Bi_{1.7}Pb_{0.3}Sr_2Ca_2Cu_3O_x$ sample has been prepared from the high purity powder of B_2O_3, PbO, $SrCO_3$, $CaCO_3$ and CuO by using the conventional solid state reaction method. The dc electrical resistivity measurements were carried out using standard four point method on BSCCO

[a] e-mail: kilic_a@ibu.edu.tr

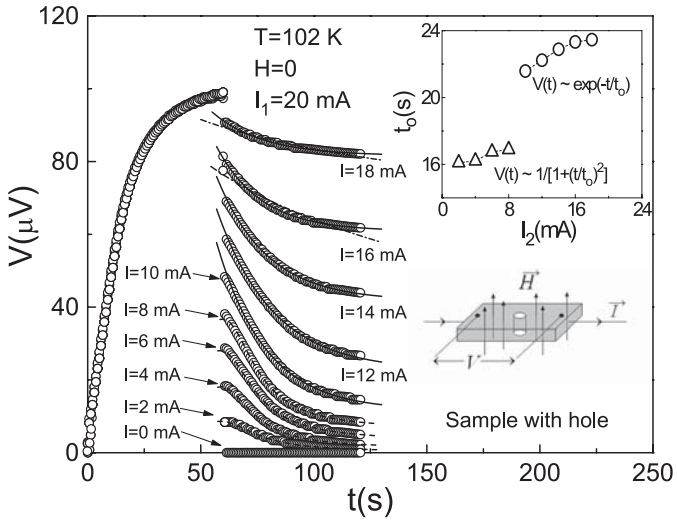

Fig. 1. $V - t$ curves of sample with hole as a function of I_2 with $I_1 = 20$ mA at $T = 102$ K and $H = 0$. Solid lines are the calculated curves of $V(t) \sim \exp(-t/t_o)$. The dashed lines with dot represent the curves calculated by $\sim\ln(t/t_o)$. The dashed lines are the best fits of the equation $V(t) \sim 1/[1+(t/t_o)^2]$. The inset in main panel represents the variation of the characteristic time t_o with current I_2.

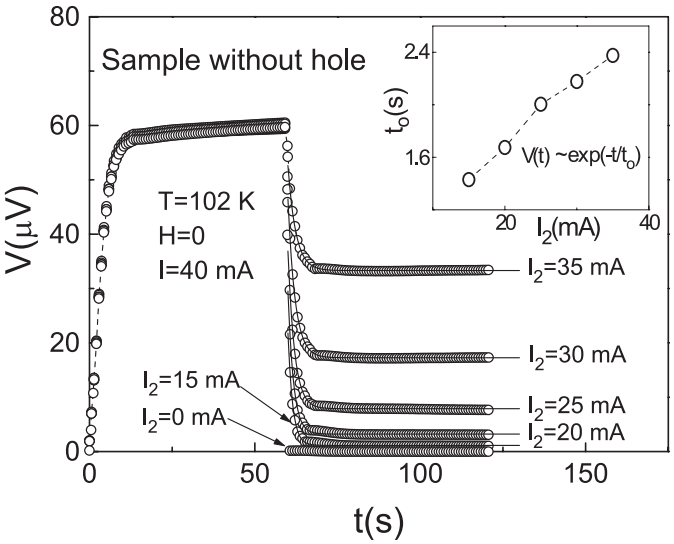

Fig. 2. $V - t$ curves of sample without hole as a function of I_2 with $I_1 = 40$ mA at $T = 102$ K and $H = 0$. Solid lines are the calculated curves of $V(t) \sim \exp(-t/t_o)$. The inset in main panel represents the variation of the characteristic time t_o with current I_2. The arrows in figure show the points belonging to the critical time (t_c) values.

sample with dimensions of length $l \sim 6.35$ mm, width $w \sim 3.4$ mm, thickness $d \sim 1.3$ mm in a closed cycle refrigerator [Oxford Instruments (OI), CCC1104]. In the experiments, Keithley-2182A with a resolution 1 nV and Keithley-6221 were used in measuring the sample voltage and applying the current, respectively. The measured voltage is the average value of 5 readings for each data point. The temperature was recorded by a calibrated 27 Ohm Rhodium-Iron thermocouple (OI, Calibration number 31202), and a temperature stability better than 10 mK were maintained during the experiments (OI, ITC-503 temperature controller). The critical temperature of BSCCO sample obtained from resistance measurements at zero field is ∼105 K and was confirmed by ac susceptibility measurements by using a SQUID magnetometer (QUANTUM DESIGN, MPMS XL) with drive field amplitude of 1 Oe and frequency of 5 Hz. The magnetic field was generated by an electromagnet (OI, N100). In $V - H$ curves, the external magnetic field (H) was oriented parallel to the axis of CH and perpendicular to the transport current ($\vec{H} \perp \vec{I}$) as shown inside Figure 1.

The time evolution of voltage ($V - t$ curves) was measured for dc currents. After the current is applied, just at this time, we start to measure the developing voltage across the sample as a function of time. Thus, monitoring of all details of the time evolution including the transient effects becomes available. In our measurements, to create a quenched state, the dc current was interrupted or reduced to a finite value: a dc driving current I_1, was applied to the sample and maintained for sometime (i.e., 60 s) to achieve a steady state. Then, the current was reduced from I_1 to a lower value, I_2, during course of the measurement, and this value kept at rest of the relaxation process, (i.e., up to 120 s). In the mean time, the sample voltage was recorded continuously.

3 Results and discussion

Figure 1 shows the $V - t$ curves of sample with hole at $T = 102$ K and at zero field ($H = 0$) on the time interval of 0–120 s. Measurements were performed for different current values of $I_2 = 0$, 2, 4, 6, 8, 10, 12, 14, 16, and 18 mA with an initial current of $I_1 = 20$ mA. $V - t$ measurements described in Figure 1 were repeated similarly for sample without hole at 102 K and $H = 0$. Figure 2 represents the $V - t$ curves of sample without hole measured with $I_1 = 40$ mA for the current values of $I_2 = 0$, 15, 20, 25, 30 and 35 mA. The non-linear growth in $V - t$ curves represented in Figures 1 and 2 can be attributed to the global reorganization of transport current which includes complex flow patterns in the volume of the sample as the time progresses [8]. In this process, the transport current (or associated vortices) penetrates into the sample from the edges and creates many channels consisting of resistive regions by first suppressing locally the superconducting order parameter in the regions where the superconductivity is weak. After this step, the moving entity will move from the sample edges towards the center along the weak pinning centers (i.e., easy motion channels). As the time progresses, the measured dissipation enhances for all $V - t$ curves, which can be considered as a measure of increase in the resistive flow channels depending on the structural disorder of sample. However, for sample with hole, the current dependent reorganization will be different because of presence of CH. At early times of relaxation

process, the transport current (or associated vortices) will try to avoid the CH by flowing around it due to the macroscopic shielding currents circulating around the periphery of the hole within a distance comparable to effective penetration depth λ [5]. Note that the measured dissipation for the $V-t$ curves of sample with hole tends to increase over time before the initial current is interrupted or reduced to a finite value. This can imply that the dynamic process concerning the reorganization of driving current is still active, so that, in one hand, the current induced flux lines penetrate and nucleate inside CH and, in the other hand, some of them leave and contribute to the measured dissipation.

In both Figures 1 and 2, when $I_2 = 0$, the sample voltage becomes zero and no trace of relaxation effects is observed. This indicates that there is no residual voltage on the sample to be relaxed within the time response of the experimental set-up [8]. When I_1 is reduced to I_2, first, an abrupt drop in voltage of sample with hole is observed, and, then, the quenched state which depends on the magnitude of I_2 decays over time. That is, the abrupt drop in voltage results in a state of quenched disorder created by I_2 and can be correlated to the supercooling of the steady state of the moving entity if one assumes that the driving current plays the role of temperature as in usual sense in statistical mechanics [2,9]. Note that the relaxation of quenched state is not smooth, but, evolves in the form of steps which continue for some time. However, in the $V-t$ curves of sample without hole, time evolution of quenched state is quite smooth up to a critical time value, t_c, marked in Figure 2, which depends on the amplitude of I_2. Finally, for $t > t_c$, we note that the response levels off at long times of relaxation process. The step wise behavior seen in $V-t$ curves belonging to sample with hole (see Fig. 1) can be related to the leaving of quantized magnetic flux lines induced by the transport current through the area of CH and to the surface superconductivity effects concerning relative enhancement of the superconducting order parameter near the hole edge.

The nature of voltage decays seen in both Figures 1 and 2 can be described by some current models. According to the modified flux flow and also the resistive weak-link models [10,11], the decrease of sample voltage in transport relaxation measurements follows a logarithmic time dependence, $\sim\ln(t/t_o)$, where t_o is the characteristic time. The dashed lines with dot in Figure 1 represent the calculated curves fitted to the data corresponding $I_2 = 18$ and 16 mA. Note the large deviation between the data and $\sim\ln(t/t_o)$ behavior. On the other hand, some experimental observations give an evidence that the glassy state relaxation fits a stretched exponential time dependence of $\sim\exp(-t/t_o)^\alpha$ on long time scales and describes the time decay in the remanent magnetic moment, where both the characteristic time t_o and the exponent α depend on current and temperature [8,12]. In this expression, the time evolution and degree of ordering of individual magnetic moments can be determined via the exponential term [8,12]. We now show that the decrease in voltage at the currents of $I_2 > 8$ mA in Figure 1 may be described

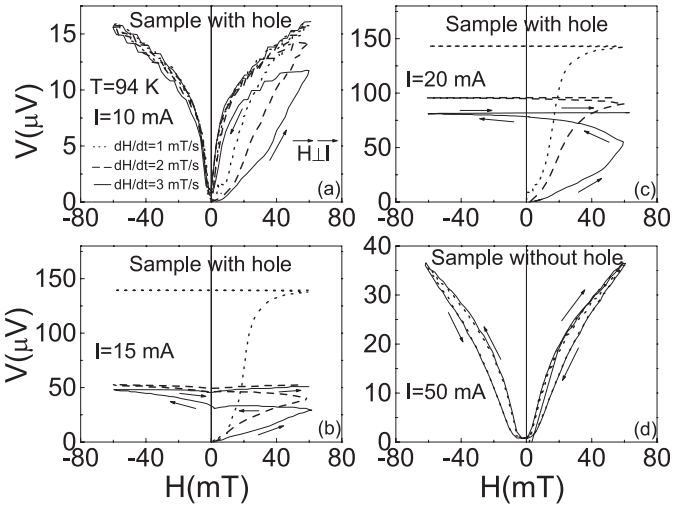

Fig. 3. (a)–(c) $V-H$ curves of sample with hole at different values of $dH/dt = 1$, 2, 3 mT/s and for $I = 10$, 15, 20 mA at 94 K, respectively. (c) $V-H$ curves of sample without hole for $I = 50$ mA at 94 K and $dH/dt = 1$ and 3 mT/s. The arrows show the direction of sweeping of external magnetic field.

by an empirical relation of $V(t) \sim \exp(-t/t_o)$ which is analogous to glassy state relaxation [8]. Solid lines in Figure 1 and Figure 2 represent the curves calculated by using $\exp(-t/t_o)$ and show reasonable agreements. The characteristic time t_o values found from the fitting of exponential relation to the data points are given in the insets of Figures 1 and 2 (open circles) as a function of I_2. It is seen from this figure that t_o tends generally to increase with I_2. This should be expected since the transitions at low currents are much faster than that of the higher ones. In fact, a quenched disorder in the moving entity can be created by interrupting abruptly the drive or reducing it to a finite value. The voltage decays in time, whatever they fit one of the relations given above, should include structural disorder due to the frustrated superconducting domains coupled by weak links and quenched disorder created in the moving entity. However, below 10 mA, the $V-t$ curves in Figure 1 give more reasonable agreement with an empirical relation of $V(t) \sim 1/[1+(t/t_o)^2]$ [11] rather than $V(t) \sim \exp(-t/t_o)$, (see the dashed lines in Fig. 1). This expression describes well the voltage hump at onset of the relaxation process after the initial current I_1 is switched to I_2. The t_o values found from the fitting procedure are given in the inset of Figure 1 (open triangles) as a function of I_2. We suggest that the voltage hump seen at the currents below 8 mA can originate from the presence of the trapped flux induced by driving current inside CH.

Figures 3a–3c show the magnetovoltage ($V-H$ curves) measurements of sample with hole taken for different field sweep rates of $dH/dt = 1$, 2, and 3 mT/s with $I = 10$, 15, and 20 mA at $T = 94$ K. In the figures, the arrows show the direction of sweeping of the magnetic field. As can be seen, both the form of $V-H$ curves and measured dissipation strongly depends on dH/dt. This implies that variation of dH/dt serves to control the number of flux

lines inside the sample and also inside CH, so that this causes a large difference between measured dissipations corresponding to 1 mT/s and 3 mT/s, respectively. It can be suggested that, at low sweep rates, the flux lines find enough time for penetration and thus an increase in the number of flux lines joining the motion causes an enhancement in measured dissipation. In addition, field sweep rate dependence shows that the number of the flux lines inside the sample and CH for each $V-H$ curve is not equal to each other. As dH/dt decreases, the effective number of flux lines through the sample with hole increase and cycling of magnetic field brings strong reversible behavior observed in $V-H$ curves depending on magnetic field and current (Figs. 3b and 3c).

Figure 3d represents the $V-H$ curves corresponding to the sample without hole for $dH/dt = 1$ and 3 mT/s at $T = 94$ K and $I = 50$ mA. It is seen that the $V-H$ curves are independent of ramping rate of field so that they collapse nearly on the same curve. This suggests that, due to the weak pinning properties of BSCOO (sample without hole), the rate of increase of field can be comparable to the time needed for the flux lines to move in the medium. In addition, the $V-H$ curves in Figure 3d reveal typical clockwise hysteretic curves for HTSC samples. The hysteresis effects are mainly related to the return flux going through the grain boundaries and generated by the trapped field in the grains [13,14]. This could explain the usual clockwise hysteretic effects in Figure 3d. However, the $V-H$ curves in Figures 3a–3c exhibit counter clockwise behavior which is unusual and we suggest that this case can originate from contribution of the flux trapped in CH to the measured dissipation as the magnetic field is decreased.

A normal region in the form of a cylinder (metallic or insulating) or a cylindrical hole attracts the flux lines since a flux line try to save core energy when it is centered at the defect, provided that the radius of the defect (r) is greater than the effective coherence length (ξ) i.e. $r > \xi$. Mkrtchyan and Shmidt (MS) [15] showed that the number of maximum flux lines, n_s, which can be trapped inside the columnar defect being as an empty cylindrical cavity is proportional to $\sim r/2\xi(T)$. In our case, the radius (r) of CH drilled in BSCCO sample is $r = 0.25$ mm and satisfies the condition of $r \gg \xi$. Thus, it should set an attractive potential energy to an incoming flux line, and, thus, should trap a large number of flux lines as compared to that of a microhole. Substituting the reasonable values of $r = 2.5 \times 10^{-4}$ m, $\xi \sim 1$ nm for BSCCO, we find that $n_s \sim 10^5$. On the other hand, the magnetic flux Φ through the area of CH can be found from the expression of $\Phi = H_s\Phi_o$ or $n_c\Phi_o$. Here n_c is the number of the flux lines and H_s is the external magnetic field where the $V-H$ curves saturate. Using $H_s \sim 60$ mT (see Fig. 3c, the $V-H$ curve taken for $I = 20$ mA) and $\Phi_o \sim 2 \times 10^{-15}$ Tm^2, we find that $n_c \sim 10^6$, so that $n_c > n_s$. This rough calculation shows that CH has a higher filling capacity than the one predicted by MS, where a single CH with the condition of $r \ll \lambda$ is considered. This may be related to the formation of multiple-quanta vortices inside CH [16–18]. Buzdin [16] showed analytically that multiple-quanta vortices on columnar defects becomes energetically favorable provided that $r^3 < \xi(T)\lambda(T)^2$. For a macroscopic CH, however, it is clear that this condition is not satisfied as in our case and it seems that the finding of $n_c > n_s$ does not originate from the presence of two-quanta (or more than this) vortices inside CH. Thus, it can be suggested that, during cycling of external magnetic field, one can rule out both formation of multiple-quanta vortices and their breaking up single quanta vortices, and their contribution to the measured dissipation. We suggest that the finding of $n_c > n_s$ can originate from substantial attractive potential energy of macroscopic CH and high degree compressibility of flux lines due to large elastic modulus C_{11} [19] as compared to a microscopic columnar defect (or microscopic hole). In the presence of CH, the energy of the Abrikosov vortex per unit length can be written as $E_v = [\Phi_o/4\pi\lambda]^2 \ln(\lambda/r)$, where Φ_o is the flux quantum, λ is the penetration depth [20]. Since $r \gg \xi$ and $E_V < 0$, CH exerts an attractive potential to the flux lines and this allows the vortices to penetrate the hole at a field which is smaller than the bulk lower critical field.

As the field is decreased, due to the field gradient evolving in the volume of the sample, the flux trapped inside CH can penetrate the sample so that CH behaves as a flux reservoir. Such a case can enhance the measured dissipation developing in the direction of driving current and can lead the saturation of sample voltage at high fields by enhancing the reversibilities in $V-H$ curves (see Figs. 3b and 3c). Thus, mobile flux lines reach an equilibrium state (i.e., correlated flux motion). We note that cycling of external magnetic field in forward and reverse directions with different sweep rates causes to increase the number of the flux lines joining the motion in both inside CH and remaining part of sample, which results in a pronounced asymmetry observed in $V-H$ curves in Figures 3a–3c.

4 Conclusion

In this paper, it was shown that relaxation of flux trapped in a macroscopic cylindrical hole (CH) drilled in a type-II superconductor could be monitored by creating a quenched state via slow transport relaxation measurements ($V-t$ curves). We observed that the time evolution of quenched state develops in the form of several pronounced steps which are correlated to leaving of quantized flux through CH and to surface superconducting effects. It was found that the voltage decays at high currents are consistent with an exponential relation which is analogous to glassy state relaxation. We also performed magnetovoltage measurements ($V-H$ curves) at different field sweep rates (dH/dt) of external magnetic field which allows to investigate the effect of a macroscopic CH on the evolution of the flux dynamics. It was observed that $V-H$ curves become strongly dH/dt dependent at a fixed transport current exhibiting remarkable time effects so that low values of dH/dt enhances considerably

the measured dissipation leading to a correlated flux motion. Furthermore, it was observed that asymmetric $V-H$ curves represent counter clockwise hysteresis effects upon cycling of the external magnetic field. This unusual observation gives an evidence of flux trapping inside CH that sets an attractive potential energy for flux lines.

This work was supported by Abant Izzet Baysal University–Dept. of Scientific Research Projects under the contract 2004.03.02.200.

References

1. Z.L. Xiao, E.Y. Andrei, M.J. Higgins, Phys. Rev. Lett. **83**, 1664 (1999)
2. K. Kiliç, A. Kiliç, H. Yetiş, O. Çetin, Phys. Rev. B **68**, 144513 (2003)
3. W. Gerhauser, G. Reis, H.W. Neumüller, W. Schmidt, O. Eibl, Saemann-Ischenko, S. Klaumünzer, Phys. Rev. Lett. **68**, 879 (1992)
4. S. Hébert, V. Hardy, G. Villard, M. Hervieu, Ch. Simon, J. Provost Phys. Rev. B **57**, 649 (1997)
5. R. Wördenweber, P. Dymashevski, V.R. Misko, Phys. Rev. B **69**, 184504 (2004)
6. A.V. Silhanek, S. Raedts, M.J. Van Bael, V.V. Moshchalkov Phys. Rev. B **70**, 054515 (2004)
7. J. Van de Vondel, C.C. de Souza Silva, B.Y. Zhu, M. Morelle, V.V. Moshchalkov Phys. Rev. Lett. **94**, 057003 (2005)
8. K. Kiliç, A. Kiliç, A. Altinkok, H. Yetiş, O. Çetin, Y. Durust, Physica C **420**, 1 (2005)
9. Y. Paltiel, E. Zeldov, Y.N. Myasoedov, H. Shtrikman, S. Bhattacharya, M.J. Higgins, Z.L. Xiao, P.L. Gammel, D.J. Bishop, Nature **403**, 398 (2000)
10. J. Wang, K.N.R. Taylor, D.N. Matthews, H.K. Liu, G.J. Russel, S. X. Dou, Physica C **180**, 307 (1991)
11. K. Kiliç, A. Kiliç, H. Yetiş, O. Çetin, J. Appl. Phys. **95**, 1924 (2004)
12. K.A. Müller, M. Takashiga, J.G. Bednorz, Phys. Rev. Lett. **58**, 1143 (1987)
13. A. Palau, T. Puig, X. Obradors, E. Pardo, C. Navau, A. Sanchez, A. Usoskin, H.C. Freyhardt, L. Fernandez, B. Holzapfel, R. Feenstra Appl. Phys. **84**, 230 (2004)
14. A. Kiliç, K. Kiliç, H. Yetiş, O. Çetin New J. Phys. **7**, 212 (2005)
15. G. Mkrtchyan, V. Shmidt Sov. Phys. JETP **34**, 195 (1972)
16. A. I. Buzdin, Phys. Rev. B **47**, 11416 (1993)
17. A. Bzeryadin, Yu.N. Ovchinnikov, B. Pannetier, Phys. Rev. B **53**, 8553 (1996)
18. M.M. Doria, G.F. Zebende Phys. Rev. B **66**, 064519 (2002)
19. E.H. Brandt, Rep. Prog. Phys. **58**, 1465 (1995)
20. A.A. Abrikosov, *Fundamentals of the Theory of Metals* (North-Holland, Amsterdam, 1988)